Cardiovascular Research Advance Access published August 8, 2013

Super-resolution fluorescence microscopy of the cardiac connexome reveals plakophilin-2 inside the connexin43 plaque

Esperanza Agullo-Pascual,[1] Dylan A. Reid,[2] Sarah Keegan[2,3], Manavjeet Sidhu,[1] David Fenyö*[2,3], Eli Rothenberg*[2,] Mario Delmar*[1]

The Leon H Charney Division of Cardiology,[1] and the Department of Biochemistry and Molecular Pharmacology,[2] Center for Health Informatics and Bioinformatics,[3] New York University School of Medicine.

*** To whom correspondence should be addressed.**

Address correspondence to:

Mario Delmar MD PhD
The Leon H Charney Division of Cardiology
New York University School of Medicine
522 First Avenue. Smilow 805
New York NY 10016 Phone (212)263-9492
Email: mario.delmar@nyumc.org

Eli Rothenberg PhD
Department of Biochemistry and Molecular Pharmacology
New York University School of Medicine
522 First Avenue. Smilow 805
New York NY 10016
Email: eli.rothenbreg@nyumc.org

David Fenyö, PhD
Center for Health Informatics and Bioinformatics
Department of Biochemistry and Molecular Pharmacology
New York University School of Medicine
227 East 30th Street, Room 739
New York NY 10016
Email: david@fenyolab.org

ABSTRACT

Aims: Cell function requires formation of molecular clusters localized to discrete subdomains. The composition of these interactomes, and their spatial organization, cannot be discerned by conventional microscopy given the resolution constrains imposed by the diffraction limit of light (~200-300 nm). Our aims were: 1) Implement single-molecule imaging and analysis tools to resolve the nanoscale architecture of cardiac myocytes. 2) Using these tools, to map two molecules classically defined as components “of the desmosome” and “of the gap junction,” and define their spatial organization.

Methods and Results: We built a setup on a conventional inverted microscope, using commercially-available optics. Laser illumination, reducing and oxygen scavenging conditions were used to manipulate the blinking behavior of individual fluorescent reporters. Movies of blinking fluorophores were reconstructed to generate sub-diffraction images at ~20 nm resolution. With this method, we characterized clusters of connexin43 (Cx43) and of “the desmosomal protein” plakophilin-2 (PKP2). In about half of Cx43 clusters, we observed overlay of Cx43 and PKP2 at the Cx43 plaque edge. siRNA-mediated loss of Ankyrin-G expression yielded larger Cx43 clusters, of less regular shape, and larger Cx43-PKP2 subdomains. The Cx43-PKP2 subdomain was validated by a proximity ligation assay (PLA) and by Monte-Carlo simulations indicating an attraction between PKP2 and Cx43 .

Conclusions: 1) Super-resolution fluorescence microscopy, complemented with Monte-Carlo simulations and PLAs, allows study of the nanoscale organization of an interactome in cardiomyocytes. 2) PKP2 and Cx43 share a common hub that permits direct physical interaction. Its relevance to excitability, electrical coupling and ARVC, is discussed.

INTRODUCTION

Proper cell function requires formation of molecular clusters at discrete subdomains. The composition of these interactomes, and their spatial organization, cannot be discerned by conventional microscopy. In-cell demonstration of physical proximity between two molecules ("co-localization") is hindered by the limited resolution of fluorescence microscopy (~200-300 nm[1]). Antibody-based co-precipitation of molecules fails to determine whether associations are direct or indirect, and involves the loss of cellular compartments. Overall, conventional co-localization or co-precipitation does not resolve whether two molecules are within range of direct interaction (<40 nm). Proximity ligation assays (PLAs) help identify molecular vicinity, but the physical characteristics of the clusters are not defined, given the diffraction limit of light. A recent breakthrough is the development of "super-resolution" fluorescence microscopy (SRFM) techniques[2] that utilize imaging, chemical and analytical tools to improve resolution into the range previously reserved for electron microscopy. Recent studies report the use of SRFM in cardiac myocytes to study sarcomeric and dyadic complexes[3-5]. Here, we combine SRFM and Monte-Carlo simulations to characterize the shape, dimensions, physical proximity and likelihood of co-localization of two proteins of the intercalated disc at a resolution of ~20 nm.

Our studies focus on two molecules fundamental to intercellular communication: connexin43 (Cx43), and plakophilin-2 (PKP2). PKP2 is classically defined as a desmosomal molecule, necessary for cell-cell adhesion, whereas Cx43 is the primary component of gap junctions. As defined by electron microscopy, desmosomes and gap junctions are distinct electron-dense structures. This has led to the notion that molecules "of the desmosome" and "of the gap junction" cannot physically interact. Yet, evidence indicates that molecules of these two complexes can cross-talk.[6-9] Thus, we speculate that though Cx43 and PKP2 populate discrete locations (desmosomes and gap junctions), they also share a common hub that permits direct physical interaction and from which they exert "non-canonical" functions[10]. The relation between

PKP2 and Cx43 is seen as key in the pathogenesis of arrhythmogenic right ventricular cardiomyopathy (ARVC), an important cause of sudden death in the young[11].

The formation of functional domains at the membrane is orchestrated, at least in part, by scaffolding molecules that couple the cytoskeleton to integral membrane proteins. A case in point is Ankyrin-G (AnkG), which supports assembly of adhesion points in epithelial cells[12], and of sodium channel clusters in neurons and heart[13, 14]. Recently, we showed that loss of AnkG expression leads to decreased electrical coupling and intercellular adhesion strength in heart cells[15]. This suggests that AnkG participates in formation of a complex involving both electrical and mechanical junctions. Yet, the limited resolution of conventional methods prevented further analysis of such complex.

Here, we implemented SRFM and Monte-Carlo simulations to define, for the first time, the morphology of immuno-reactive Cx43 and PKP2 clusters in intact cells. We demonstrate that the outer edge of Cx43 plaques is also populated by PKP2, and that the dimensions of these clusters depend on AnkG expression. The existence of a Cx43-PKP2 subdomain was confirmed using a proximity ligation assay (PLA) both in culture monolayers, and in adult ventricular tissue. We propose that the Cx43-PKP2 subdomain is a shared, interactive hub (a “connexome”) for molecules that control excitability, adhesion and intercellular communication in the heart.

METHODS

Neonatal rat ventricular myocytes (NRVMs) were dissociated from hearts of 3-4 day old rats, euthanized by decapitation and removal of the heart, following standard procedures[9]. Conditions for cell culture, Western blot, immunofluorescence microscopy and shRNA-mediated loss of AnkG expression were as in[15]. PLA protocols were adapted from previous publications[16] and from the manufacturer's instructions. For adult mouse cardiac tissue, we used thin (2-3 µm) sections. Mice were euthanized with an anaesthetic overdose (isoflurane >20%) and confirmed death by cervical dislocation. All procedures were in accordance with New York University guidelines (IACUC Protocol 101101-02 to MD approved on 7 November 2011) for animal use and care and conformed to the Guide for the Care and Use of Laboratory Animals published by the US National Institutes of Health (NIH Publication 58-23, revised 1996).

SRFM

Super-resolution imaging was done using a custom-built fluorescence microscope (Leica DMI3000) configured for total internal reflection fluorescence (TIRF) and highly inclined excitation (HILO) modes. The microscopy methods, related calibrations and controls are detailed in the online supplement and Online Figure 1 (see also references[17 18-22]). Cluster analysis was performed using ImageJ software, (see also online supplement).

Monte-Carlo simulations

Simulations were used to define the likelihood and magnitude of signal overlap in an environment where a) two independent molecular species were randomly and uniformly distributed or b) an attraction variable between Cx43 and PKP2 (a "co-localization factor") was included. Further details are in online supplement.

RESULTS

SRFM

SRFM has been used for nanoscale localization of proteins in subcellular compartments[3-5, 23]. Here, we adapted it for the first time to explore the association between intercalated disc molecules. NRVMs were fixed and prepared as for conventional immunofluorescence microscopy. Cx43 and PKP2 were immunolocalized using commercially available antibodies and Alexa fluorophores (A568 and A647 for Cx43 and PKP2, respectively). Figure 1 shows an image of a site of intercellular contact obtained by conventional TIRF before (A) and after image reconstruction (B). Small white squares in (A) outline areas enlarged in (C), (D) and (E). Panels C and D show diffused diffraction limited resolution of the TIRF image (left), and improved clarity after reconstruction (right). Panel E shows an enlarged super-resolved image, highlighting physical characteristics consistently observed: A semi-circular Cx43 cluster (green), a neighboring PKP2 cluster of less defined shape (purple), and an edge of Cx43 where two clusters overlap (white). Panel F shows a topological image, with signal intensity represented in the z-axis. Values of fluorescence amplitude for each protein cluster along a cross-section of the image (dotted line) are plotted in (G). Notice the Gaussian shape of the Cx43 intensity plot, intersected by the PKP2 intensity curve, creating an area of overlap. These overlap areas were seen on the edges of Cx43 plaques, and not in their center; we did not observe instances where Cx43 surrounded the PKP2 signal. In contrast to normal distribution of fluorescence intensity across Cx43 clusters, many PKP2 intensity plots were non-Gaussian, displaying long plateaus interrupted by dips, likely reflecting two or more separate clusters, too close to be discerned.

Physical characteristics of Cx43- and PKP2-immunoreactive protein clusters in cardiac cells.

Super-resolved images (as in 2A) were used to measure area, perimeter and circularity of clusters, as well as intensity profiles. As shown in 2B, the area occupied by individual Cx43

clusters ranged from 8,000 to 88,000 nm^2, but the histogram revealed two primary peaks, both defined by Gaussian functions: one with an average value of 13,313±328 nm^2 (+/- SEM) and the other one, at 25,035±227 nm^2. The two peaks were statistically different from one another, with the mean value of the first Gaussian corresponding to near half the mean value of the second Gaussian. Clusters were mostly circular, with a circularity index larger than 0.8 for 65.4% of all clusters examined (2C). As shown in 2D and 2E, there was close correlation between area and perimeter of clusters, and between perimeter and circularity, with clusters of smaller dimension being of more circular shape. Clusters with circularity larger than 0.8 were used to characterize fluorescence intensity profiles across the diameter (average plot in 2F). Amplitude was normalized to maximum observed in each cluster and distances measured relative to peak of the Gaussian curve. Consistently, Cx43 fluorescence intensity increased progressively from periphery to center, suggesting that Cx43 density is highest in the plaque center and less toward the periphery, in agreement with freeze-fracture images of gap junction plaques[24]. Results like those described in Figure 2 were found in cells treated with oligonucleotides that do not affect expression of relevant proteins (ϕshRNA; see[15]; data in supplemental Figure 2). The physical features of Cx43 clusters contrasted with those of PKP2 plaques, which displayed a much broader distribution of area and circularity (Supplemental Figure 3A-D), consistent with the idea that PKP2 plaques may be formed by more than one cluster, in very close apposition to each other. Given that limitation, the rest of the quantitative analysis was explored from the perspective of the Cx43 plaques.

PKP2-immunoreactive molecules populate the Cx43 cluster: The shared Cx43-PKP2 subdomain.

The ability to co-localize fluorescently labeled immuno-reactive proteins with enhanced spatial resolution allowed us to examine proximity of Cx43 to PKP2 (Figure 3A). Figure 3B displays a histogram of distances separating the edge of Cx43 clusters from the closest edge of a PKP2

plaque. Notice that the largest column corresponds to cluster distances of less than zero, i.e., where the edge of the PKP2 plaque is inside the Cx43 cluster. Overall, 41.9% of Cx43 clusters showed some degree of overlay with PKP2. This result was opposite to the conventional expectation that Cx43 and PKP2 belong to distinct, separate domains of the myocyte. Similar results were observed in cells treated with a non-silencing construct (ϕshRNA; panel 3C). In that case, 57.6% of Cx43 clusters intersected a PKP2 plaque. Figure 3D shows a plot correlating area covered by the Cx43-PKP2 subdomain (ordinates), with size of the corresponding Cx43 cluster (abscissa). Black or red circles correspond to clusters measured from untreated (UNT) or ϕshRNA-treated cells, respectively. Identity line (slope of 1) demarcates upper limit of co-localization, i.e., the point at which PKP2 would occupy the entire Cx43 cluster area. The dotted line (slope of 0.5) indicates 50% co-localization. We observed primarily two data groups: The first, contained between the identity line and its 50% reference, showed a relation between Cx43 cluster size and co-localization area (area in light gray). The second one, corresponded to cases where the co-localization area remained below 10,000 nm^2 regardless of Cx43 cluster size (light blue). As expected from measurements of Cx43 cluster size (Figure 2 and supplemental Figure 2), most data points were contained within the 8,000 to 60,000 nm^2 range. Next, we assessed whether these parameters depended on AnkG expression[15]. Treatment with a non-silencing construct (ϕshRNA) did not affect the measured parameters and as such, data from UNT and ϕshRNA-treated cells were combined.

Physical characteristics of the Cx43 clusters depend on AnkG expression

NRVMs were treated with oligonucleotides that prevent AnkG expression (AnkG-shRNA). Western blots confirmed that shRNA treatment prevented AnkG expression (e.g., supplemental Figure 4). Figure 4A shows frequency distribution of Cx43 cluster areas in AnkG-silenced cells (red histogram). Gaussian functions describing the control data set are shown as a black line,

for comparison (from data in Figure 2B). The first Gaussian peak in the AnkG-silenced group, centered at 16,613 ± 322 nm^2, was similar to the first Gaussian peak measured in control (see Figure 2). However, a second Gaussian population was not clearly defined. In fact, cluster areas distributed broadly, with areas larger than ~25,000 nm^2. In fact, while 12.3% of the clusters in the control group fell outside the 8,000 to 60000 nm^2 range, there was a larger fraction of clusters larger than 60,000 nm^2 in the AnkG silenced group (26.9% of the total). Loss of AnkG expression also correlated with increased number of clusters with a low circularity index (59.9 %; panel B).

AnkG expression limits the size of the Cx43-PKP2 subdomain

As shown in supplemental Figure 5, loss of AnkG expression did not reduce the abundance of Cx43 clusters per unit area, but decreased abundance of PKP2 plaques per unit area. Nonetheless, the frequency of Cx43 clusters sharing a subdomain with PKP2 remained similar to control. Indeed, of a total of 381 Cx43 clusters analyzed, 54.6% did not show overlap with PKP2 (a proportion similar to that in control group; see Figure 3). On the other hand, the size of the Cx43-PKP2 co-localization area was significantly affected by the absence of AnkG. Figure 4C shows the plot correlating area of each Cx43 cluster (abscissa), with that of the corresponding Cx43-PKP2 shared subdomain (ordinates) measured from cells treated with AnkG-shRNA. For reference, the light gray and light blue regions, demarcating areas of this plot occupied by control data, are also depicted. (Same areas as in 3D; notice difference in scales.) Clearly, Cx43 clusters in cells lacking AnkG expression showed a wider range of sizes, and the area of co-localization with PKP2 also varied in a wider range. In fact, 40.6% of points in the plot in 4C are outside the windows populated by the control data. These results illustrate the power of SRFM to define nano-scale changes in molecular distribution relevant to intercellular communication.

Monte-Carlo simulations define and quantify the attraction between Cx43 and PKP2

Experimental work was complemented with Monte-Carlo simulations. We first compared the experimentally-observed Cx43-PKP2 co-localization, with a model in which clusters of the same size, shape and density were randomly placed within a similar area of detection. Supplemental Figures 6-9 compare the physical characteristics of the simulated clusters, with those detected experimentally. Figure 5A shows a sample image from the simulations. In contrast to experimental observations (Figures 3-4), only 20% and 22% of Cx43 clusters simulating control and AnkG silenced cells, respectively, overlapped with a PKP2 cluster. Moreover, the extent of overlap of randomly assigned clusters showed a different profile from that recorded experimentally. Analysis was based on plots of Cx43-PKP2 co-localization as a function ofCx43 cluster area (i.e., Figures 3D and 4C). We separated the data into three groups: points that fell between the identity line and 50% overlap (0.51 to 1.0), between 10 and 50% overlap (0.1 to 0.5), and less than 10% overlap (<0.1). Experimental data are shown in red and modeled data, in blue. Notice the disparity between modeled and experimental results (Fig.5B). While the model predicted a similar probability density along the 0.1 to 1.0 range, experimental data showed a much higher frequency of events (probability density) for co-localization in the 0.5 to 1.0 window. These results strongly support the notion of an attraction between Cx43 and PKP2, whereby overlap is not random. Interestingly, the data profile from AnkG-silenced cells suggests that AnkG maintains, at least in part, the attraction between Cx43 and PKP2 (Figure 5C).

The simulations above showed that a model based on random distribution did not reproduce experimental data. Complementarily, we hypothesized a better experimental-model convergence if Cx43 and PKP2 were treated as mutual attractors (model details in online supplement). Figures 5D-G show the probability density for co-localization as a function of a "co-localization factor," where f=1 was the random condition, and f=32 was the highest co-

localization factor tested (further details in online methods). Panel 5D shows results based on the probability density for co-localization in the 0.5-1.0 range in control conditions, and panel 5F, in the AnkG-silenced cells. Corresponding data for probability density in the 01-0.5 range are shown in 5E and 5G. In all cases, the green line indicates the value recorded from the experiments (red bars in 5B and 5C). Notice that the model data progressively approached the experimental value once the co-localization factor was increased and in fact, in the case of AnkG, the plots intersected. These results indicate that Cx43-PKP2 co-localization is not random, and loss of AnkG expression decreases the extent of attraction between the two molecules.

Cx43 and PKP2 co-localization demonstrated by a proximity ligation assay (PLA)

The existence of a shared Cx43-PKP2 space in the intercellular junction interactome was confirmed by PLAs[16]. The tissue was exposed to two antibodies, one recognizing Cx43 and the other one, PKP2, and the two antibodies were ligated and labeled with a single fluorophore. A third antibody was used to detect Cx43 molecules that did not react in the PLA. As shown in Figure 6A, we observed abundant Cx43-PKP2 co-localization. Quantification of the number of PLA-positive spots, in relation to those only immuno-reactive to the Cx43 antibody is shown in 6B. Finally, to prove that the area of Cx43-PKP2 overlap is also a confined subdomain of the adult intercalated disc, we implemented PLAs in sections of mouse cardiac ventricle. As shown in 6C, we detected a frequent PLA signal (blue) in the intercalated disc, especially in the direction perpendicular to the long axis of the cells. Cx43 was also detected intermingled with PLA-positive spots. Interestingly, in areas where Cx43 aligned parallel to fiber direction, PLA signals were conspicuously absent, suggesting that Cx43 and PKP2 overlap primarily at the intercalated disc.

DISCUSSION

We have used a novel fluorescence microscopy method to localize two cardiac junctional proteins, Cx43 and PKP2, with a spatial resolution previously reserved to the electron microscope. As opposed to EM, where only electron-dense structures can be discerned, SRFM allows for localization of protein clusters using conventional fluorescent-labeled antibodies. A combination of chemical, optical and analytical manipulations results in identification of the fluorescence source with a spatial resolution that breaks the barrier imposed by the Abbe diffraction limit, estimated at ~250 nm (see[25] for review on SRFM). In our case, resolution between separate points was ~20 nm, yielding the first co-localization of Cx43 and PKP2-immunoreactive proteins in cardiac cells at the nanometer scale. We demonstrate that PKP2 and Cx43 are not confined to separate structures but rather, they can overlap in space. The methodological innovation also involved Monte-Carlo simulations to validate and characterize the attraction between PKP2 and Cx43. This is the first study demonstrating the existence of a shared Cx43-PKP2 subdomain within the boundaries of a Cx43 plaque. We also show that the dimensions of this domain, and of the entire Cx43 cluster, are restricted by AnkG expression.

Characteristics of Cx43 clusters

Our data showed that most Cx43 clusters are of two defined dimensions: One of approximately 25,000 nm^2 and the other one of ~half that size. A third group corresponded to larger clusters, though not larger than ~ 90,000 nm^2. In the Cx43 life cycle, at least three types of Cx43 aggregates can be found at or near the membrane: a connexon, a gap junction, and the "connexosomes," representing large Cx43-rich membrane vesicles. We speculate that the three sizes correspond to each of those stages. Interestingly, loss of AnkG, known to decrease junctional conductance[15], associated with decreased amplitude of the second Gaussian peak. Additional experiments will be needed to confirm the relation between cluster size, and functional state.

Interaction of Cx43 with PKP2 and with AnkG

As stated in online methods, we calculated the final axial imaging volume after rejection in our set-up to be equal or less than 160 nm. In the X-Y plane, when considering only Cx43 clusters within the two Gaussians in Fig.2B, average cluster diameter was ~150 nm. The circular XY projections originated from 3-dimensional gap junction plaques, likely raising several tenths of nanometers in the z plane. Similarly, PKP2 plaques occupied a large area (see suppl.Fig.3) and likely represent a volume where clusters raise several tenths of nanometers on the z plane. We show overlap of Cx43 and PKP2 signals. That is, at least part of Cx43 and PKP2 clusters occupy the same axial imaging volume. Considering the size of each individual cluster, and our knowledge on the dimensions of gap junction and desmosome plaques, it is unlikely that our results are consequent to the presence of a desmosome standing on top of a gap junction, both fitting within the axial imaging volume after rejection without reaching an interactive range. Rather, our results argue in favor of the idea that PKP2 is present within the confines of a Cx43 plaque.

We demonstrated that the spatial domain of a Cx43 plaque often includes PKP2 molecules. This is consistent with data showing PKP2 and Cx43 in the same precipitate. Yet, we also showed that a fraction of Cx43 plaques did not contact PKP2. We speculate that the Cx43-PKP2 association occurs only within a given window of the Cx43 plaque life cycle, The characteristics of such association are not known. What is clear is that PKP2 expression and/or structural integrity is necessary to preserve gap junctions[6].

AnkG is a cytoskeletal adaptor protein. In the heart, as in other structures such as the nodes of Ranvier[26], AnkG couples the pore-forming alpha subunit of the sodium channel to the actin

cytoskeleton[13]. In cardiac myocytes, AnkG co-precipitates and functionally interacts with Cx43[15]. Here, we show that loss of AnkG expression allowed formation of large Cx43 plaques. This is reminiscent of the observation in myelinated axons, where Na_V -associated scaffolding proteins act as barriers to restrict invasion of flanking paranodal domains[27]. We propose that AnkG flanks and restricts Cx43 cluster size. Interestingly, loss of AnkG expression leads to decreased electrical coupling between cells[15]. This inverse relation between Cx43 plaque size and Cx43-mediated electrical coupling supports the notion that only a fraction of Cx43 forms functional gap junctions, and such a fraction can be regulated independently from factors that control plaque size.

Defining Cx43 subdomains: the perinexus and the "connexome."

Regulation of Cx43 plaque size has been extensively studied for zonula occludens-1 (ZO-1). Recent studies showed that Cx43-ZO-1 association occurs in the periphery of the Cx43 plaque (the "perinexus")[16] and that loss of ZO-1 interaction leads to larger gap junction plaques, with loss of perinexus space. Here, we report that loss of AnkG caused increased abundance of plaques of larger size. Yet, this manipulation also caused reduced electrical coupling[15]. We speculate that AnkG and ZO-1 are mutually exclusive, so that the perinexal space is restricted by the presence of AnkG at its border (Figure 6D). Accordingly, loss of AnkG would allow expansion of the perinexus, increasing Cx43-ZO-1 contact area and thus, further limiting access of Cx43 to the inner core of the plaque, where gap junctions are formed (Figure 6D, right panel).

The functional consequences of associations in the perinexus likely extend beyond formation of electrical or mechanical junctions. Recent studies show non-canonical, gap junction-independent functions of Cx43[10]. Key among them is preservation of sodium current amplitude[28] [29]. In fact, mutations in Cx43 can cause ventricular arrhythmias and sudden death even when electrical coupling is preserved[30]. PKP2 also regulates amplitude and gating behavior of the

sodium current[9]. The observation that both $Na_V1.5$[31] and PKP2 are in physical contact with Cx43 leads us to suggest that the Cx43 plaque hosts a molecular complex (a "connexome") that regulates electrical coupling, cell adhesion and cell excitability..

The connexome and ARVC pathogenesis

The existence of PKP2 as part of the connexome is contrary to the perception of PKP2 as a component of mechanical junctions that only interact with Cx43 in a distant, and indirect manner. The possibility of direct Cx43-PKP2 cross-talk is relevant to the molecular pathophysiology of ARVC (or AC; see[32]). Mutations in PKP2 are the most common cause of familial ARVC. Loss of Cx43 plaques is a common finding in ARVC-affected hearts[11] and in cells lacking PKP2[6]. The mechanism by which a "desmosomal molecule" such as PKP2 leads to loss of Cx43 plaques, has puzzled investigators. Our data show that the cause of PKP2-dependent loss of Cx43 plaques does not need to be indirect. These molecules are likely direct partners, co-inhabitants of a physical space, and the structural integrity of one is likely to be necessary for the preservation of the other and of the connexome as a whole. Our results provide a novel angle to better understand the relation between sequence integrity of PKP2, and occurrence of deadly arrhythmias in young patients, even in the absence of overt structural disease[32].

Sources of Funding

Supported by grants from National Institutes of Health (R01-HL106632 and R01-GM57691 to M.D, and U54-RR02220 to D.F.), and Leducq Foundation Transatlantic Network (M.D).

Conflict of interest: none declared

REFERENCES

1. Born MW, E. Principles of Optics: Electromagnetic Theory of Propagation, Interference and Diffraction of Light. *Cambridge University Press* 1997.

2. Heilemann M, van de Linde S, Schuttpelz M, Kasper R, Seefeldt B, Mukherjee A*, et al.* Subdiffraction-resolution fluorescence imaging with conventional fluorescent probes. *Angew Chem Int Ed Engl* 2008;**47**:6172-6176.

3. Baddeley D, Jayasinghe ID, Lam L, Rossberger S, Cannell MB, Soeller C. Optical single-channel resolution imaging of the ryanodine receptor distribution in rat cardiac myocytes. *Proc Natl Acad Sci U S A* 2009;**106**:22275-22280.

4. Soeller C, Baddeley D. Super-resolution imaging of EC coupling protein distribution in the heart. *J Mol Cell Cardiol* 2013;**58**:32-40.

5. Wong J, Baddeley D, Bushong EA, Yu Z, Ellisman MH, Hoshijima M*, et al.* Nanoscale Distribution of Ryanodine Receptors and Caveolin-3 in Mouse Ventricular Myocytes: Dilation of T-Tubules near Junctions. *Biophys J* 2013;**104**:L22-24.

6. Oxford EM, Musa H, Maass K, Coombs W, Taffet SM, Delmar M. Connexin43 remodeling caused by inhibition of plakophilin-2 expression in cardiac cells. *Circ Res* 2007;**101**:703-711.

7. Asimaki A, Tandri H, Huang H, Halushka MK, Gautam S, Basso C*, et al.* A new diagnostic test for arrhythmogenic right ventricular cardiomyopathy. *N Engl J Med* 2009;**360**:1075-1084.

8. Li J, Patel VV, Kostetskii I, Xiong Y, Chu AF, Jacobson JT*, et al.* Cardiac-specific loss of N-cadherin leads to alteration in connexins with conduction slowing and arrhythmogenesis. *Circ Res* 2005;**97**:474-481.

9. Sato PY, Musa H, Coombs W, Guerrero-Serna G, Patino GA, Taffet SM*, et al.* Loss of plakophilin-2 expression leads to decreased sodium current and slower conduction velocity in cultured cardiac myocytes. *Circ Res* 2009;**105**:523-526.

10. Agullo-Pascual E, Delmar M. The noncanonical functions of Cx43 in the heart. *J Membr Biol* 2012;**245**:477-482.

11. Kaplan SR, Gard JJ, Protonotarios N, Tsatsopoulou A, Spiliopoulou C, Anastasakis A*, et al.* Remodeling of myocyte gap junctions in arrhythmogenic right ventricular cardiomyopathy due to a deletion in plakoglobin (Naxos disease). *Heart Rhythm* 2004;**1**:3-11.

12. Kizhatil K, Davis JQ, Davis L, Hoffman J, Hogan BL, Bennett V. Ankyrin-G is a molecular partner of E-cadherin in epithelial cells and early embryos. *J Biol Chem* 2007;**282**:26552-26561.

13. Lowe JS, Palygin O, Bhasin N, Hund TJ, Boyden PA, Shibata E*, et al.* Voltage-gated Nav channel targeting in the heart requires an ankyrin-G dependent cellular pathway. *J Cell Biol* 2008;**180**:173-186.

14. Zhou D, Lambert S, Malen PL, Carpenter S, Boland LM, Bennett V. AnkyrinG is required for clustering of voltage-gated Na channels at axon initial segments and for normal action potential firing. *J Cell Biol* 1998;**143**:1295-1304.

15. Sato PY, Coombs W, Lin X, Nekrasova O, Green KJ, Isom LL*, et al.* Interactions between ankyrin-G, Plakophilin-2, and Connexin43 at the cardiac intercalated disc. *Circ Res* 2011;**109**:193-201.

16. Rhett JM, Jourdan J, Gourdie RG. Connexin 43 connexon to gap junction transition is regulated by zonula occludens-1. *Mol Biol Cell* 2011;**22**:1516-1528.

17. Henriques R, Lelek M, Fornasiero EF, Valtorta F, Zimmer C, Mhlanga MM. QuickPALM: 3D real-time photoactivation nanoscopy image processing in ImageJ. *Nat Methods* 2010;**7**:339-340.

18. Malkusch S, Muranyi W, Muller B, Krausslich HG, Heilemann M. Single-molecule coordinate-based analysis of the morphology of HIV-1 assembly sites with near-molecular spatial resolution. *Histochem Cell Biol* 2013;**139**:173-179.

19. Yamaguchi S, Reid DA, Rothenberg E, Darwin AJ. Changes in Psp protein binding partners, localization and behaviour upon activation of the Yersinia enterocolitica phage shock protein response. *Mol Microbiol* 2013;**87**:656-671.

20. Hong M, Bao L, Kefaloyianni E, Agullo-Pascual E, Chkourko H, Foster M*, et al.* Heterogeneity of ATP-sensitive K+ Channels in Cardiac Myocytes: ENRICHMENT AT THE INTERCALATED DISK. *J Biol Chem* 2012;**287**:41258-41267.

21. Chkourko HS, Guerrero-Serna G, Lin X, Darwish N, Pohlmann JR, Cook KE*, et al.* Remodeling of mechanical junctions and of microtubule-associated proteins accompany cardiac connexin43 lateralization. *Heart Rhythm* 2012;**9**:1133-1140 e1136.

22. Simonson PD, Rothenberg E, Selvin PR. Single-molecule-based super-resolution images in the presence of multiple fluorophores. *Nano Lett* 2011;**11**:5090-5096.

23. Dani A, Huang B, Bergan J, Dulac C, Zhuang X. Superresolution imaging of chemical synapses in the brain. *Neuron* 2010;**68**:843-856.

24. Palatinus JA, Rhett JM, Gourdie RG. The connexin43 carboxyl terminus and cardiac gap junction organization. *Biochim Biophys Acta* 2012;**1818**:1831-1843.

25. van de Linde S, Loschberger A, Klein T, Heidbreder M, Wolter S, Heilemann M*, et al.* Direct stochastic optical reconstruction microscopy with standard fluorescent probes. *Nat Protoc* 2011;**6**:991-1009.

26. Kordeli E, Lambert S, Bennett V. AnkyrinG. A new ankyrin gene with neural-specific isoforms localized at the axonal initial segment and node of Ranvier. *J Biol Chem* 1995;**270**:2352-2359.

27. Thaxton C, Pillai AM, Pribisko AL, Dupree JL, Bhat MA. Nodes of Ranvier act as barriers to restrict invasion of flanking paranodal domains in myelinated axons. *Neuron* 2011;**69**:244-257.

28. Jansen JA, Noorman M, Musa H, Stein M, de Jong S, van der Nagel R*, et al.* Reduced heterogeneous expression of Cx43 results in decreased Nav1.5 expression and reduced sodium current that accounts for arrhythmia vulnerability in conditional Cx43 knockout mice. *Heart Rhythm* 2012;**9**:600-607.

29. Desplantez T, McCain ML, Beauchamp P, Rigoli G, Rothen-Rutishauser B, Parker KK*, et al.* Connexin43 ablation in foetal atrial myocytes decreases electrical coupling, partner connexins, and sodium current. *Cardiovasc Res* 2012;**94**:58-65.

30. Lubkemeier I, Requardt RP, Lin X, Sasse P, Andrie R, Schrickel JW*, et al.* Deletion of the last five C-terminal amino acid residues of connexin43 leads to lethal ventricular arrhythmias in mice without affecting coupling via gap junction channels. *Basic Res Cardiol* 2013;**108**:348.

31. Rhett JM, Ongstad EL, Jourdan J, Gourdie RG. Cx43 associates with Na(v)1.5 in the cardiomyocyte perinexus. *J Membr Biol* 2012;**245**:411-422.

32. Delmar M, McKenna WJ. The cardiac desmosome and arrhythmogenic cardiomyopathies: from gene to disease. *Circ Res* 2010;**107**:700-714.

FIGURE LEGENDS

Figure 1: TIRF vs SRFM. NRVMs stained for Cx43 and PKP2. Panels A and B show same region of intercellular contact visualized by TIRF (A) and by super-resolution microscopy (B). Small white squares in A are enlarged in C, D and E. Panels C and D show improved resolution after reconstruction (right). Panel E: Cx43 cluster surrounded by PKP2, also shown in F as a topological image (z axis: signal intensity). Dotted line across image is plotted in G to show intersection of both signals. Scale bars: 5 μm (A, B) and 200nm (C, D, E).

Figure 2: Cx43 cluster analysis. A: Cx43 (green) and PKP2 (purple), with an area of overlap (white). Yellow dotted line demarcates area of Cx43 cluster while blue dotted line demarcates area of PKP2 cluster. B: Histogram of area occupied by each Cx43 cluster. Notice two primary Gaussian peaks centered at 13,313±328 nm^2 and 25,035±226 nm^2. C: Cluster circularity index; a value of 1.0 indicates perfect circle. D: Correlation between area and perimeter. E: Correlation between perimeter and circularity; note that smaller clusters have a more circular shape. F: Average profile of Cx43 fluorescence intensity along the diameter of Cx43 clusters with circularity index larger than 0.8. n=136 clusters of 6 images analyzed.

Figure 3: Analysis of Cx43-PKP2 subdomain. A: Example of Cx43 (green) and PKP2 (purple) localization, with an area of overlap (white). Histograms in B and C show distances between a Cx43 cluster and the closest PKP2 cluster. B: Untreated cells. C: Cells treated with a control oligonucleotide that does not prevent protein expression. In both histograms, largest number of events (41.9 and 57.6% respectively), correspond to cases where Cx43 and PKP2 overlap (represented by first bar left of “0 nm” point). D: Scatter plot correlates Cx43 cluster area with area covered by Cx43-PKP2 subdomain. Gray shade illustrates area between identity line (solid

diagonal line) and its 50% reference (dotted diagonal line); blue area highlights clusters with a co-localization of less than 10,000 nm^2. n= 124 and 66, respectively.

Figure 4: Cx43 cluster dimensions in AnkG-silenced cells. A: distribution of Cx43 cluster areas in AnkG-silenced cells (red histogram) and comparison with Gaussian functions defining Cx43 cluster areas in control (black lines). B: Cluster circularity index in AnkG-silenced cells. n=424 clusters of 12 images analyzed. C: Cx43-PKP2 subdomain in cells treated with AnkG-shRNA. Gray and blue areas defined for control cells (Figure 4D) are shown for reference. n=128 clusters.

Figure 5: Analysis of the Cx43-PKP2 subdomain by Monte-Carlo simulations. A: sample image for a simulation of Cx43 and PKP2 clusters drawn as randomly distributed ellipses over a 30,000 x 2000 nm box. B, C: Correlation Cx43-PKP2 subdomain and Cx43 cluster area of control cells and AnkG-silenced cells respectively, in experimental data (red) and modeled data (blue). Data is separated in three different groups: more than 50% overlap, 10 to 50% overlap or less than 10% overlap. D, E and F, G: probability density for co-localization between Cx43 and PKP2 as a function of a “co-localization factor”, i.e. increased Cx43-PKP2 attraction. D: Untreated cells, >50% overlap. E: AnkG-silenced cells, >50% overlap. F: Untreated cells, 10%-50% overlap. G: AnkG-silenced cells, 10%-50% overlap.

Figure 6: A: Cx43-PKP2 interaction in rat heart tissue, detected by a proximity ligation assay (Duolink). Cx43-PKP2 cross-reactivity by PLA, is shown in blue. Cx43 alone is depicted in green. Scale bar = 10μm. B: Proposed model of Cx43 plaque organization. The gap junction is surrounded by an area defined as the perinexus where Cx43 hemichannels interact with ZO-1; this interaction regulates the transition of connexons to the gap junction[16]. We speculate that AnkG is localized at the border of the perinexus; we further speculate that AnkG and ZO-1 are mutually exclusive and in this manner, AnkG restricts plaque size. When AnkG is silenced (right

panel), the area of influence of ZO-1 increases, expanding the perinexal area at the expense of the actual pore-forming gap junction, yielding larger Cx43 plaque sizes and yet, a reduced channel-forming domain.

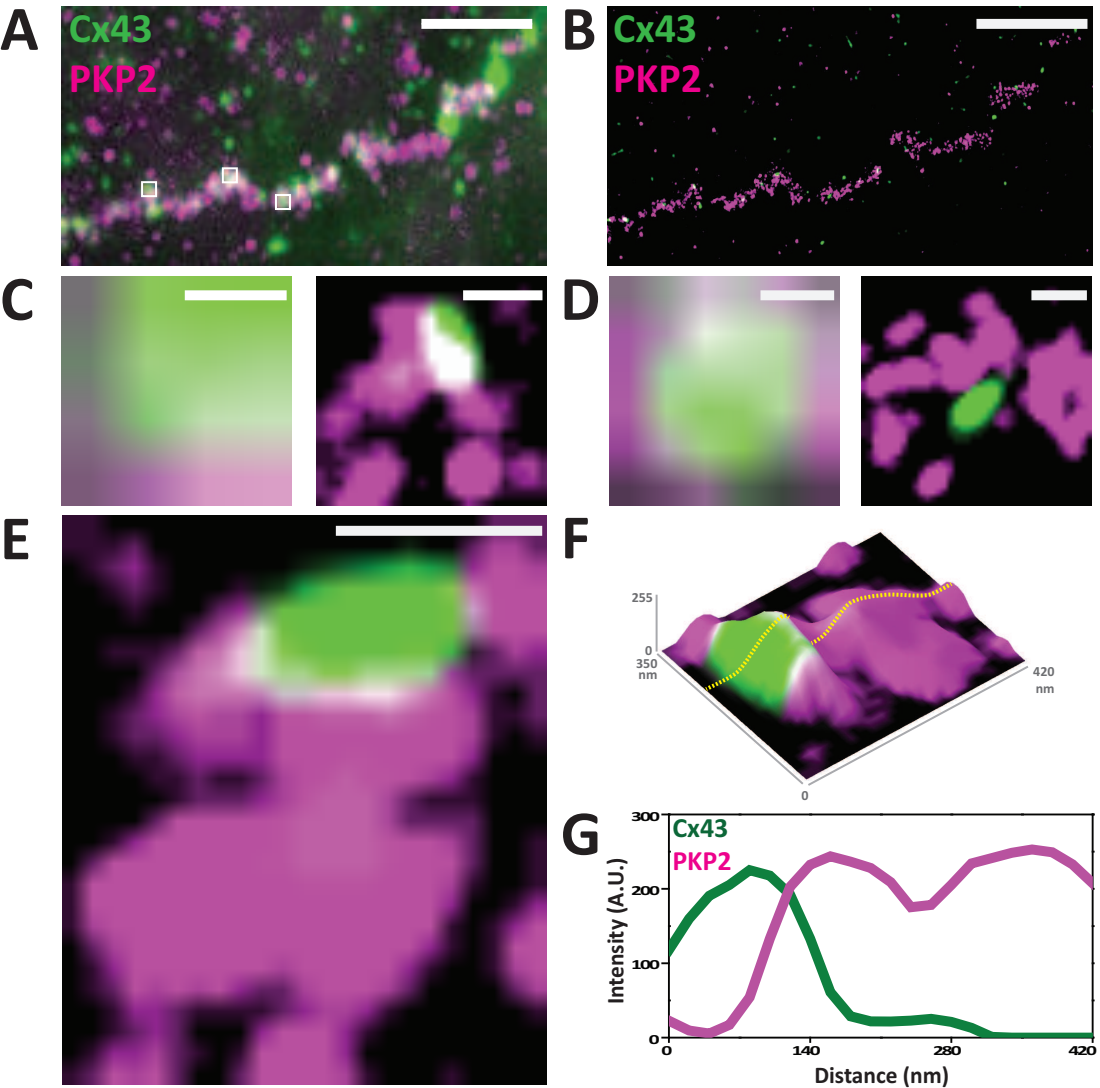

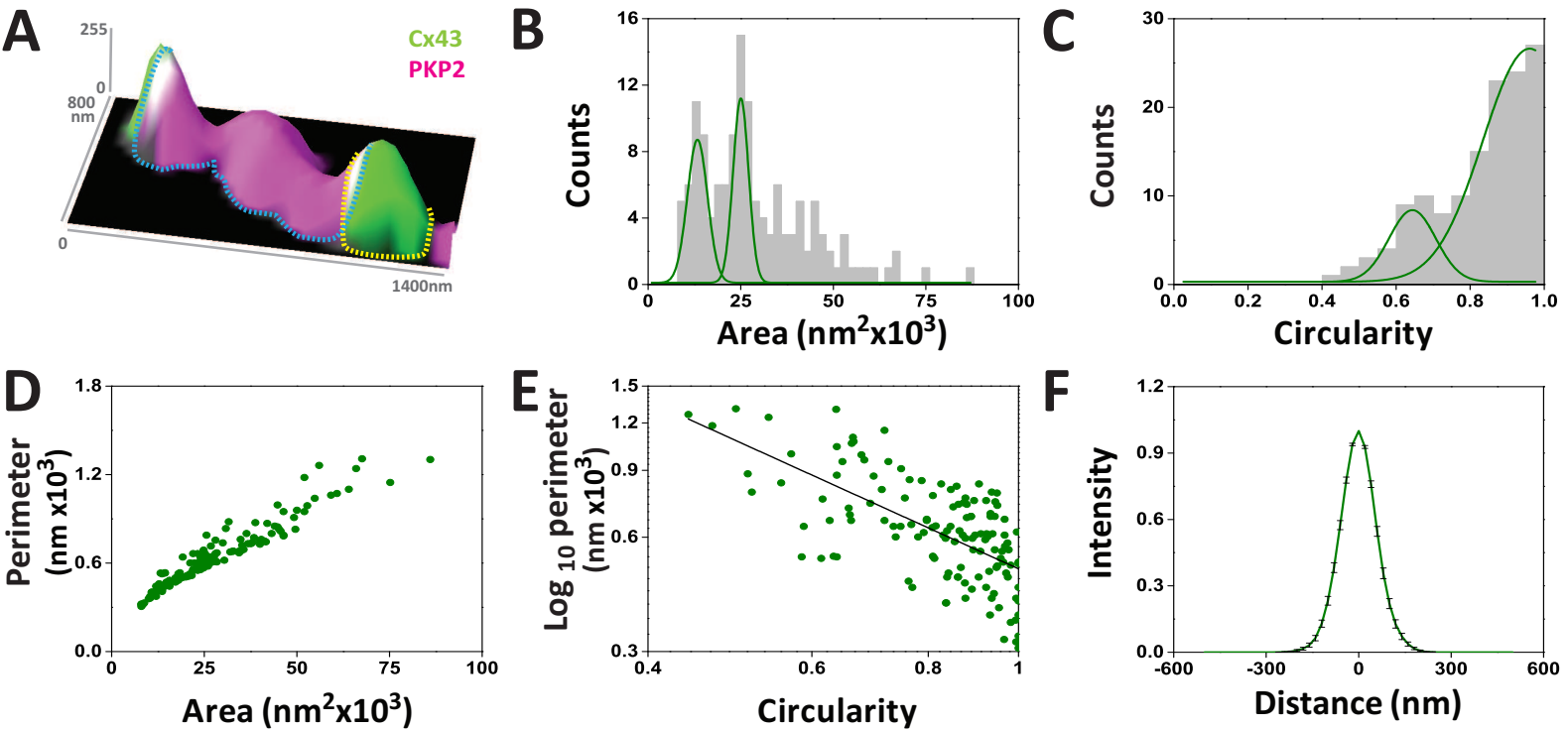

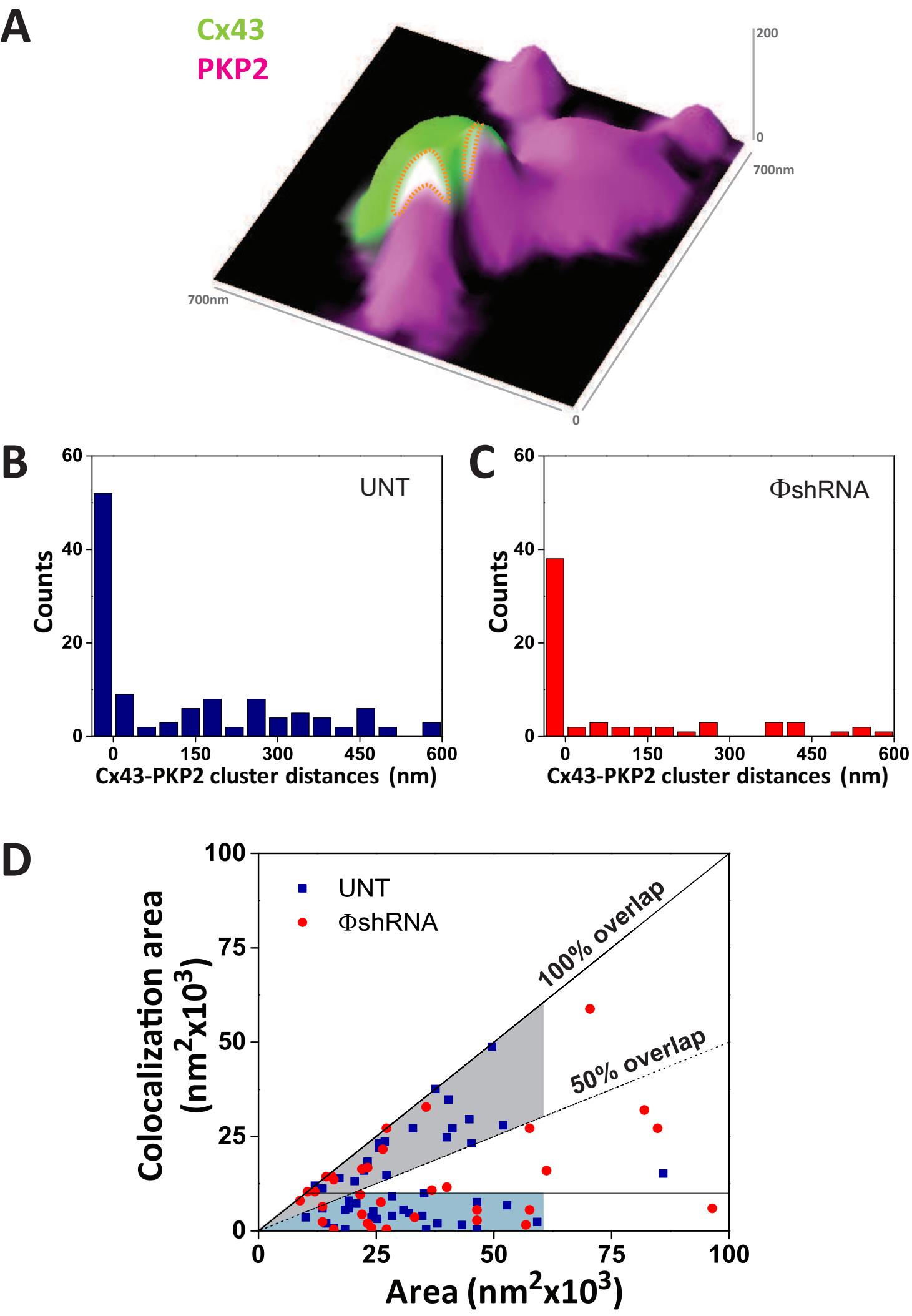

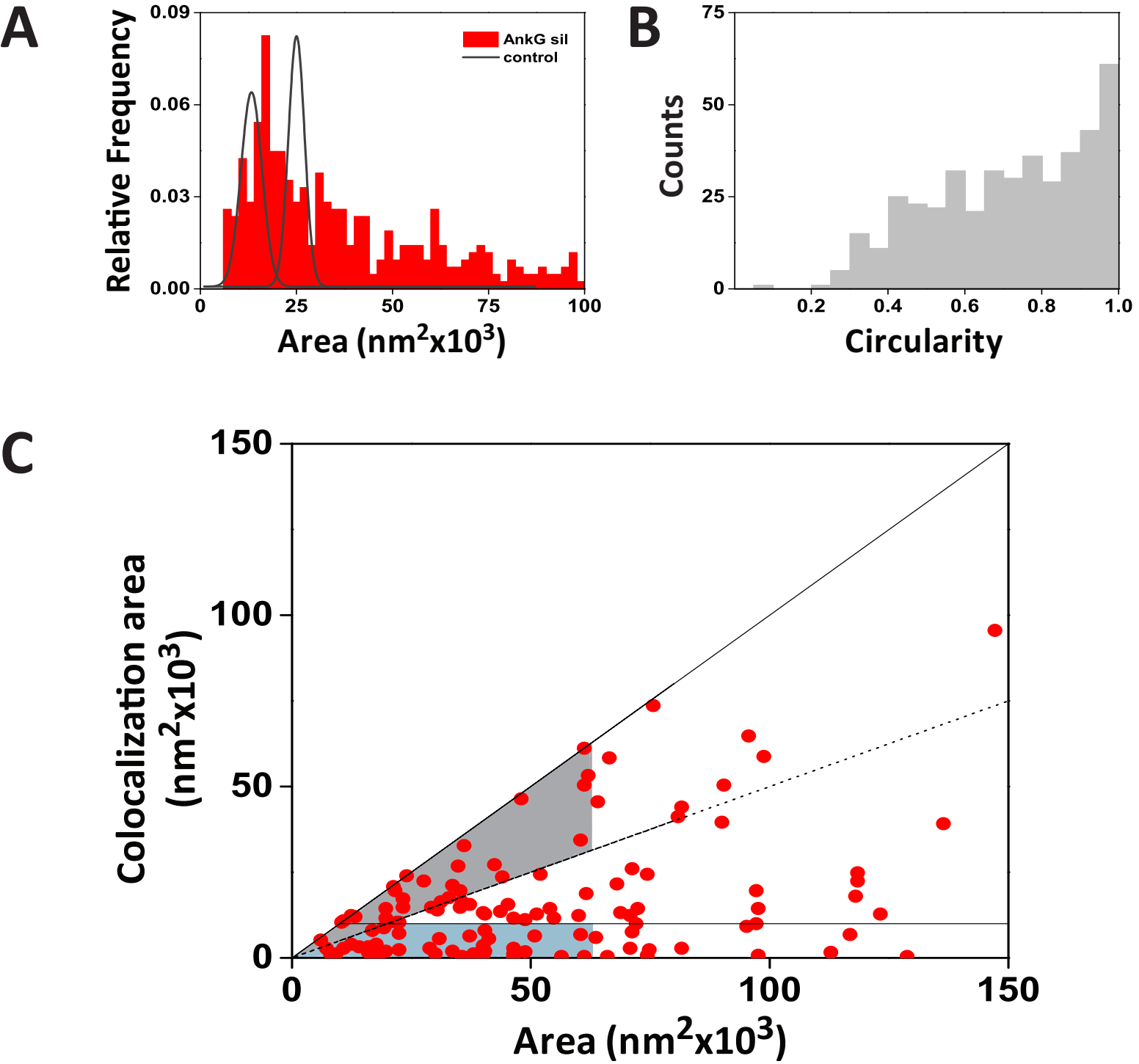

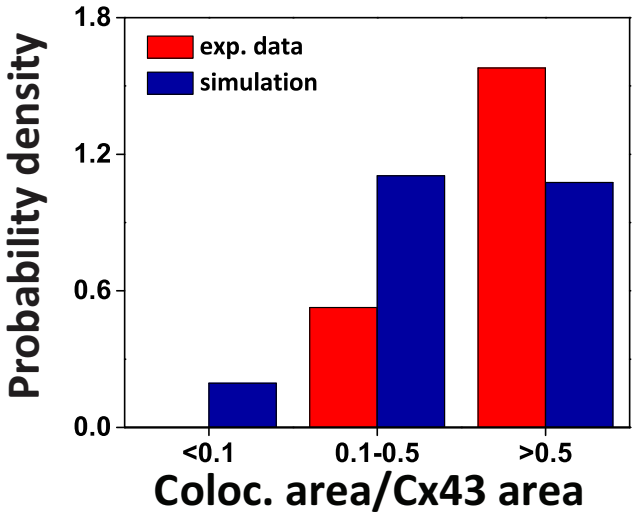

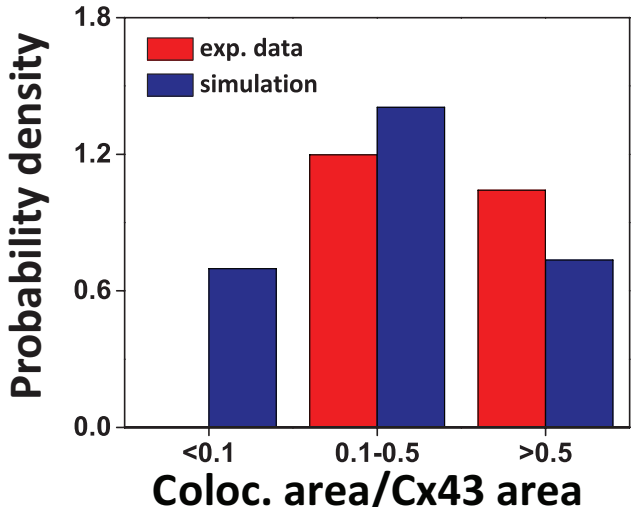

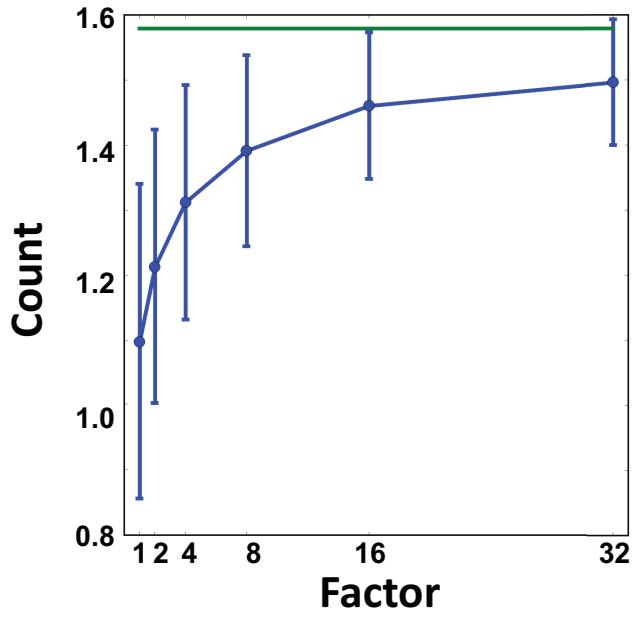

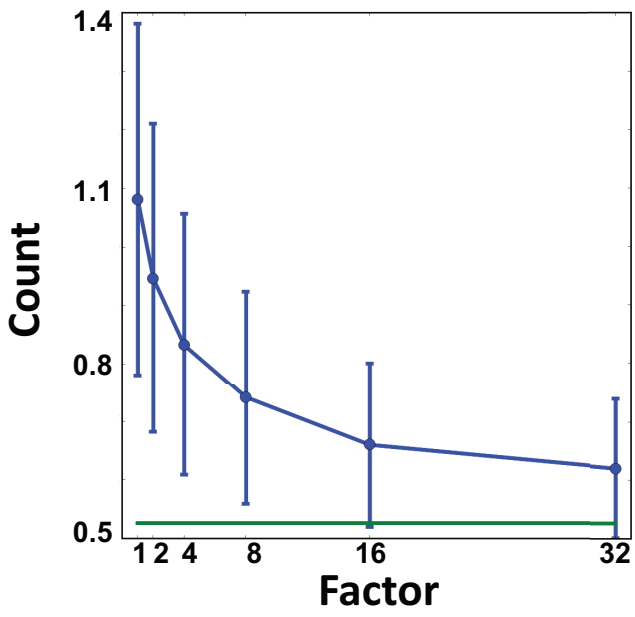

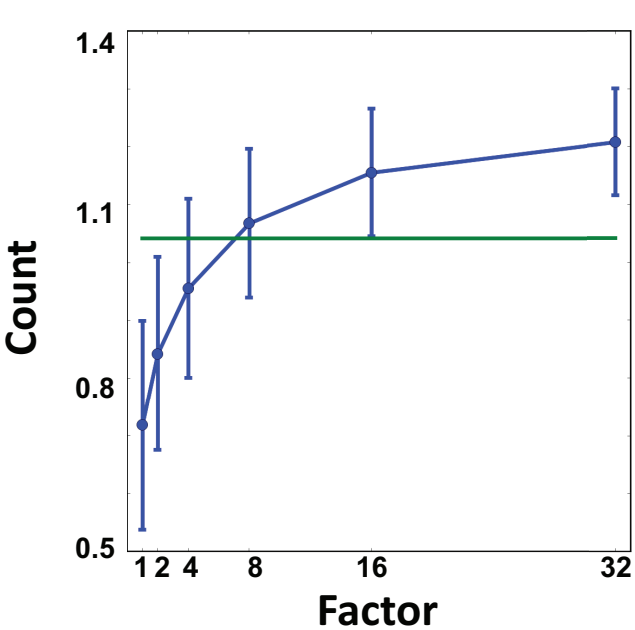

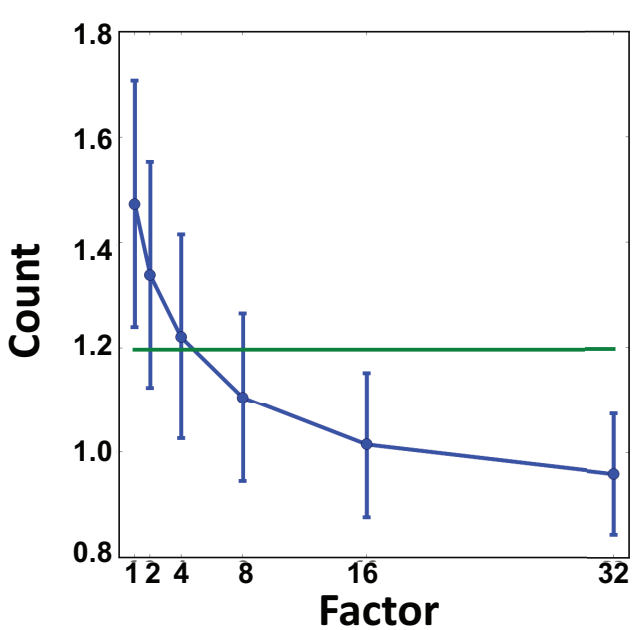

A

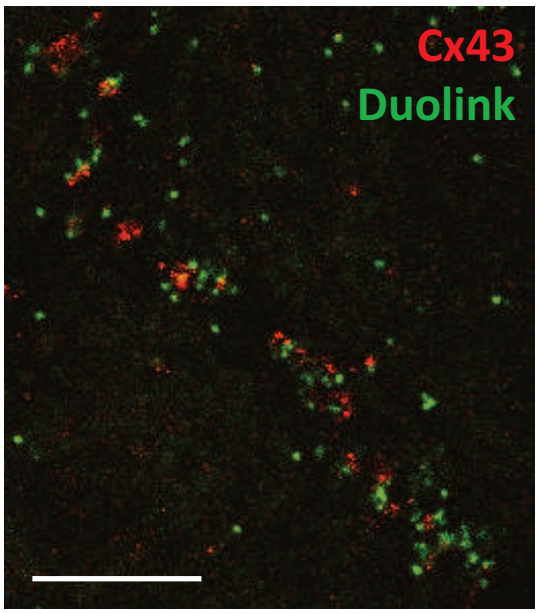

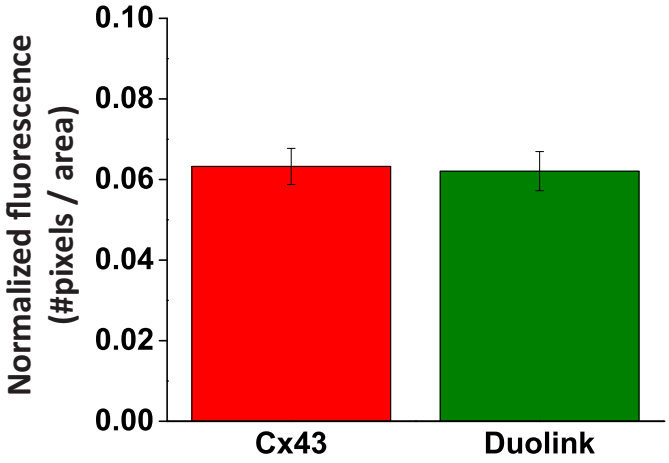

B

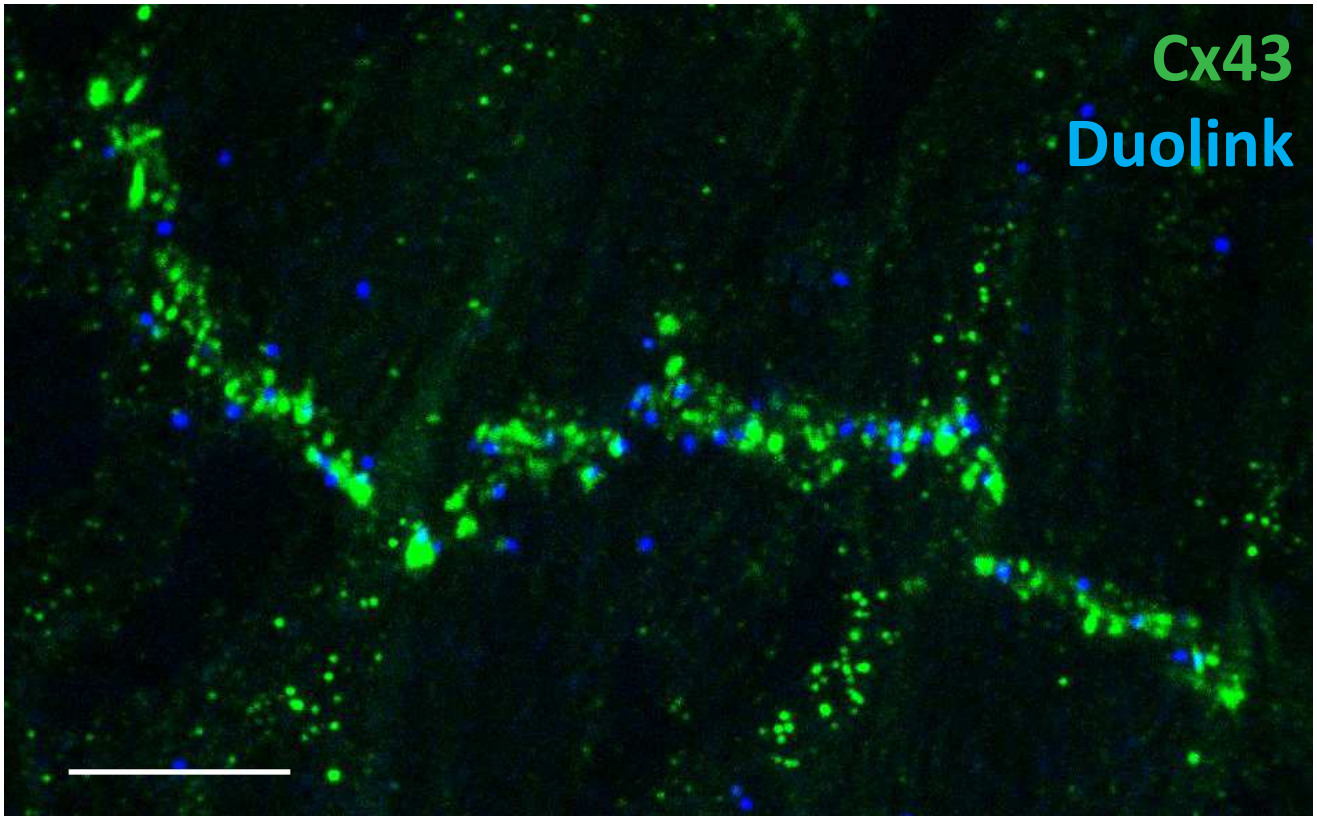

C